Research Square

Preprints are preliminary reports that have not undergone peer review.
They should not be considered conclusive, used to inform clinical practice,
or referenced by the media as validated information.

Effect of substrate temperature on the structural, optical, and photoconductive properties of co-evaporated ZnS1-xTex thin films

Camilo Andrés Velásquez Andrade

caavelasquezan@unal.edu.co

Universidade do Vale do Paraíba

Nestor Jaime Torres

Universidad Nacional de Colombia

Research Article

Keywords: ZnS1−xTex, thin films, thermal co-evaporation, band gap, photoconductivity, photodetectors

Posted Date: September 29th, 2026

DOI: https://doi.org/10.21203/rs.3.rs-11028978/v1

License: This work is licensed under a Creative Commons Attribution 4.0 International License.
Read Full License

Additional Declarations: No competing interests reported.

Effect of substrate temperature on the structural, optical, and photoconductive properties of co-evaporated $ZnS_{1-x}Te_x$ thin films

Camilo Andrés Velásquez Andrade[1,3*] and Néstor Jaime Torres[2,3]

[1*]Instituto de Pesquisa e Desenvolvimento (IP&D), Universidade do Vale do Paraíba (UNIVAP), Av. Shishima Hifumi, 2911 Urbanova, São José dos Campos, 12244-000, São Paulo, Brazil.

[2]Departamento de Física, Universidad Nacional de Colombia (UNAL), Carrera 45 # 26 85, Edif. Uriel Gutiérrez, Bogotá, 111321, Distrito Capital, Colombia.

[3]Grupo de Materiales con Aplicaciones Tecnológicas (GMAT), Universidad Nacional de Colombia (UNAL), Carrera 45 # 26 85, Edif. Uriel Gutiérrez, Bogotá, 111321, Distrito Capital, Colombia.

*Corresponding author(s). E-mail(s): caavelasquezan@unal.edu.co;
Contributing authors: njtorress@unal.edu.co;

Abstract

$ZnS_{1-x}Te_x$ thin films were deposited on glass substrates by thermal co-evaporation under high-vacuum conditions. The effect of substrate temperature on composition, crystal structure, optical properties, photoluminescence, and spectral photoconductive response was investigated. Energy-dispersive X-ray spectroscopy showed that the Te fraction varied markedly with substrate temperature, with x values of 0.90, 0.67, 0.13, and 0.39 for films deposited at 100, 150, 200, and 250 °C, respectively. X-ray diffraction revealed that the films were polycrystalline, with a cubic zinc-blende structure and preferred (111) orientation. Optical characterization showed band-gap energies ranging from 2.19 to 3.13 eV across the investigated sample series. The photoluminescence spectrum of the film deposited at 100 °C exhibited a broad emission band that was fitted with two Gaussian components centered at approximately 515 and 579 nm. Photoconductivity measurements revealed broad spectral responses that depended on substrate temperature: films deposited at 100 and 150 °C exhibited a photoconductive response over almost the entire visible range, whereas the film deposited at 250 °C showed a response shifted toward longer wavelengths. These results

demonstrate that substrate temperature provides an effective means of modifying the composition and optoelectronic response of $ZnS_{1-x}Te_x$ thin films and support further investigation of these films as potential materials for broadband visible photodetection.

Keywords: $ZnS_{1-x}Te_x$; thin films; thermal co-evaporation; band gap; photoconductivity; photodetectors

1 Introduction

II-VI compound semiconductors, including ZnS, ZnSe, and ZnTe, exhibit structural, optical, and electronic properties that make them of interest for optoelectronic applications. These materials are direct-band-gap semiconductors, and their properties can vary considerably depending on their composition, crystal structure, and growth conditions. In particular, ZnS and ZnTe represent the binary end members of the $ZnS_{1-x}Te_x$ alloy system and exhibit significant differences in their lattice constants and band-gap energies. These differences provide a basis for tailoring the optical and electronic properties of the ternary alloy through composition control [1, 2].

One strategy for broadening the range of accessible properties in II-VI compounds is to form ternary alloys such as $ZnS_{1-x}Se_x$, $ZnSe_{1-x}Te_x$, and $ZnS_{1-x}Te_x$. Studies conducted on related ternary systems have shown that structural, optical, and electrical properties can be significantly modified by varying the alloy composition [3–5]. In this context, the $ZnS_{1-x}Te_x$ system is particularly interesting due to the significant differences between the properties of its binary end members and the strong dependence of its electronic structure on the Te fraction.

Unlike a simple linear interpolation between ZnS and ZnTe, the band-gap energy of $ZnS_{1-x}Te_x$ exhibits a marked nonlinear dependence on composition. Yu et al. [6] experimentally observed strong band-gap bowing in $ZnS_{1-x}Te_x$ epitaxial layers and described its dependence on the Te fraction using $E_{g(x)} = 3.73 - 5.27x + 3.80x^2$. Seong et al. [7] also reported an anomalous variation in the band-gap with composition in this system. These results show that modifying the S/Te ratio can produce significant changes in the electronic structure and optical response of the material, beyond a simple interpolation between the binary compounds.

This dependence on composition is also evident in the emission and photodetection properties of the $ZnS_{1-x}Te_x$ system. Blue electroluminescence has been demonstrated in ZnSTe-based devices, where the isoelectronic centers associated with Te play a significant role in the emission processes [8]. Similarly, $ZnS_{1-x}Te_x$-based Schottky detectors with composition-dependent spectral sensitivity have been fabricated [9]. These findings indicate that controlling the composition is an important tool for modifying the optoelectronic response of $ZnS_{1-x}Te_x$ alloys.

In addition to the nominal composition of the precursor materials, growth conditions can significantly alter the final properties of thin films. In thermal evaporation processes, the substrate temperature can affect species incorporation, crystal structure, crystallite size, and optical and electrical properties. In ZnTe films obtained by thermal evaporation, Bacaksiz et al. [10] demonstrated that the substrate temperature influences the microstructure, crystalline quality, band-gap energy, and electrical properties. Thermal evaporation also offers a relatively simple and reproducible method for preparing thin films, in which deposition conditions can be controlled experimentally [2].

In co-evaporation processes, the final film composition may depend not only on the initial amounts of the precursor materials but also on transport and incorporation processes that are sensitive to the growth conditions. Consequently, substrate temperature may play an important role in determining the S/Te ratio incorporated during growth and, as a result, the structural, optical, and photoconductive properties of the films. Establishing these relationships is particularly important for determining the extent to which deposition conditions can be used to control the spectral response of the $ZnS_{1-x}Te_x$ system.

This study investigates the effect of substrate temperature on the composition, crystalline structure, optical properties, photoluminescence, and photoconductive spectral response of $ZnS_{1-x}Te_x$ thin films deposited on glass via thermal co-evaporation in a high vacuum. The films were prepared at substrate temperatures ranging from 100 to 250 $^{\circ}C$, while keeping the other main deposition conditions constant. The relationship between substrate temperature, alloy composition, and optoelectronic properties is analyzed to determine how growth conditions can be used to modify the material's photoconductive response in the visible region.

2 Materials and methods

2.1 Thin-film deposition and substrate preparation

$ZnS_{1-x}Te_x$ thin films were deposited on Corning glass substrates by high-vacuum thermal co-evaporation using ZnS and ZnTe powders with a nominal purity of 99.995%. The evaporation source consisted of a cylindrical furnace and a graphite Knudsen cell divided into separate chambers for the two source materials. ZnTe was placed in the lower chamber and ZnS in the middle chamber, with 85 mg of each compound loaded for each deposition. The vapors followed separate paths inside the source and were combined in an upper mixing chamber before reaching the substrate. During heating, the shutter remained closed. ZnTe evaporation began at approximately 750 $^{\circ}C$, ZnS vaporization became significant at approximately 850 $^{\circ}C$, and the source was heated to a final temperature of approximately 1000 $^{\circ}C$ before deposition. The substrates were positioned 15 cm from the evaporator outlet. Depositions were carried out for 18 min at a base pressure of approximately 1.0×10^{-5} mbar. The substrate temperature was controlled using a PID controller and was set to 100, 150, 200, or 250 $^{\circ}C$ for the films analyzed in this work. A schematic representation of the evaporation source is

shown in Figure 1a.
Glass substrates were cleaned with detergent and rinsed three times with distilled/deionized water. They were subsequently immersed in a sulfochromic solution for 24 h and ultrasonically cleaned in distilled water for 5 min; this ultrasonic-cleaning step was repeated three times. Finally, the substrates were rinsed with isopropyl alcohol and acetone and dried with hot air.

2.2 Compositional characterization

The composition of the $ZnS_{1-x}Te_x$ films was evaluated by energy-dispersive X-ray spectroscopy (EDX/EDAX) using a TESCAN VEGA3 scanning electron microscope equipped with a Bruker EDX system. Spectra were acquired for 90 s at an accelerating voltage of 25 kV, a beam-intensity setting of 10, and a magnification of 5,000×. The Bruker EDX analysis provided both normalized weight percentages (wt.%) and atomic percentages (at.%).
For determination of the alloy composition parameter x, the atomic concentrations were used. Because x in $ZnS_{1-x}Te_x$ represents the relative occupation of the chalcogen sublattice by S and Te, substrate-related contributions such as O and Si were excluded and x was calculated directly from the S and Te atomic concentrations as

$$x = \frac{C_{Te}}{(C_S + C_{Te})} \tag{1}$$

and

$$1 - x = \frac{C_S}{(C_S + C_{Te})} \tag{2}$$

where C_S and C_{Te} are the measured atomic concentrations of S and Te, respectively. Zn was retained in the elemental-composition analysis but was not included in the calculation of x. The resulting Te fractions used throughout the manuscript are x = 0.90, 0.67, 0.13, and 0.39 for films deposited at 100, 150, 200, and 250 $°C$, respectively.

2.3 Structural characterization

The crystalline structure of the films was investigated by X-ray diffraction (XRD) using a Philips XPert PRO PANalytical diffractometer in Bragg–Brentano geometry with monochromatic Cu Kα radiation ($\lambda = 1.5406$ Å). Diffraction patterns were recorded over the 2θ range from 10° to 90° using a step size of 0.02° and an acquisition time of 20 s per step. Structural identification was performed with XPert HighScore Plus by comparison with reference patterns from the Inorganic Crystal Structure Database (ICSD). ZnTe and ZnS zinc-blende reference patterns were used as structural end-member references for interpretation of the ternary alloy, rather than as evidence of two physically separated phases.
The full width at half maximum (FWHM) of the most intense diffraction peak was obtained by Gaussian fitting. The crystallite size D was estimated using the Scherrer equation

$$D = \frac{K\lambda}{\beta \cos\theta} \tag{3}$$

where $K = 0.9$ is the Scherrer constant, $\lambda = 1.5406$ Å is the X-ray wavelength, β is the FWHM expressed in radians, and θ is the Bragg angle [11]. For the cubic structure, the lattice parameter a was obtained from Bragg's law and the interplanar-spacing relation $d_{hkl} = a/(h^2 + k^2 + l^2)^{1/2}$; for the (111) reflection, $a = \sqrt{3}d_{111}$.

2.4 Optical characterization

Optical transmittance spectra were measured at normal incidence using a Varian Cary 5000 spectrophotometer over the wavelength range from 300 to 2500 nm. The film thickness, refractive index, and absorption-related optical parameters were determined from the experimental transmittance spectra using Swanepoel's envelope method [12]. The calculated film thicknesses were 772, 843, 408, and 271 nm for substrate temperatures of 100, 150, 200, and 250 °C, respectively.

The optical band gap was evaluated assuming a direct allowed transition using the Tauc relation

$$(\alpha h\nu)^2 = A(h\nu - E_g) \tag{4}$$

where α is the absorption coefficient, $h\nu$ is the photon energy, A is a proportionality constant, and E_g is the optical band gap. E_g was determined by extrapolating the linear portion of the $(\alpha h\nu)^2$ versus $(h\nu)$ plot to $(\alpha h\nu)^2 = 0$.

2.5 Photoluminescence measurements

Photoluminescence (PL) measurements were performed at room temperature using a 1000 W Hg lamp as the excitation source. The luminescence emitted by the sample was collected and directed to a monochromator through quartz optics. The spectrally resolved signal was detected with a photomultiplier tube and amplified using a current preamplifier and a lock-in amplifier. The PL analysis presented in this work corresponds to the film deposited at 100 °C ($x = 0.90$).

2.6 Photoconductivity measurements

For spectral photoconductivity measurements, Cu electrodes were deposited on the surface of the $ZnS_{1-x}Te_x$ thin films by high-vacuum thermal evaporation at a base pressure of approximately 2.5×10^{-5} mbar. The electrode configuration provided in-plane electrical conduction, with a separation of 1 mm between the parallel Cu electrodes, as shown in Fig. 1b.

Measurements were performed at room temperature using a halogen lamp as the illumination source. The light beam was spectrally selected using a monochromator with a focal length of 0.25 m (Oriel Instruments/Cienitec) and directed perpendicular to the film surface. The illuminated area on the sample was approximately 3×4 mm^2.

A bias voltage of 90 V was applied across the Cu electrodes during the measurements.

The resulting photocurrent was amplified using a current preamplifier and detected with a lock-in amplifier. The measured photoconductivity spectra were corrected for the spectral response of the measurement system.

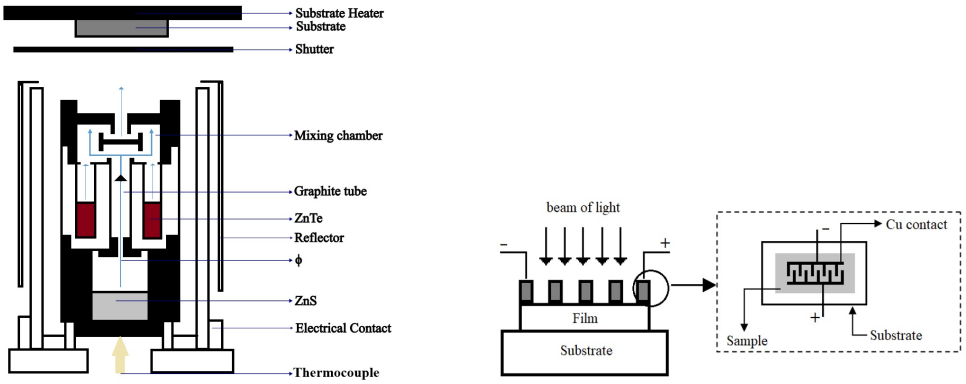

(a) (b)

Fig. 1: Experimental configuration used for thin-film deposition and photoconductivity measurements. (a) Evaporation source used for the thermal co-evaporation growth of $ZnS_{1-x}Te_x$ thin films. (b) Cross-sectional and top views of the photoconductive sample geometry, showing the Cu electrodes deposited by high-vacuum thermal evaporation with a separation of 1 mm between the parallel electrodes.

3 Results

3.1 Composition of the ternary $ZnS_{1-x}Te_x$ thin films

EDX analysis confirmed the presence of Zn, S, and Te in all $ZnS_{1-x}Te_x$ thin films. The characteristic K and L lines of Zn, the K line of S, and the L and K lines of Te were identified in the spectra. Figure 2 shows a representative EDX spectrum of the film deposited at a substrate temperature of 100 °C.

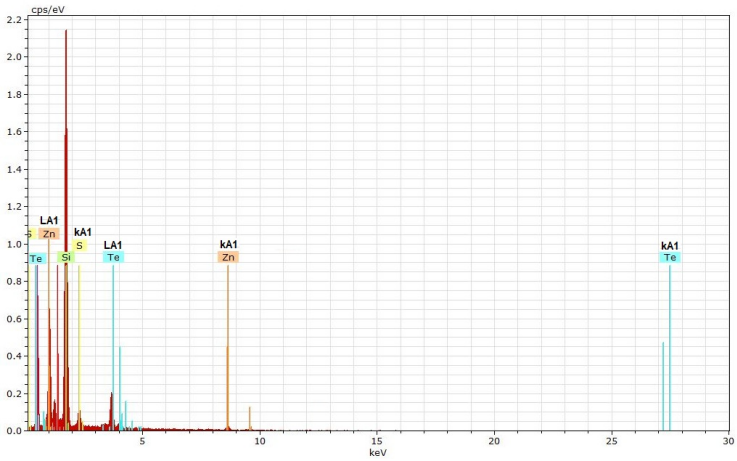

Fig. 2: Representative EDX spectrum of the $ZnS_{1-x}Te_x$ thin film deposited on a glass substrate at $T_s = 100\,°C$ ($x = 0.90$).

The alloy compositions, expressed as $ZnS_{1-x}Te_x$ using the calculated Te fraction, were $ZnS_{0.10}Te_{0.90}$, $ZnS_{0.33}Te_{0.67}$, $ZnS_{0.87}Te_{0.13}$, and $ZnS_{0.61}Te_{0.39}$ for substrate temperatures of 100, 150, 200, and 250 °C, respectively. As the substrate temperature increased from 100 to 200 $°C$, the Te concentration decreased from x = 0.90 to x = 0.13. At 250 $°C$, however, the Te concentration increased to x = 0.39.

3.2 Structural characterization

X-ray diffraction patterns showed that the $ZnS_{1-x}Te_x$ thin films were polycrystalline and crystallized in the cubic zinc-blende structure. The diffraction patterns were indexed using the ICSD reference data for ZnTe (96-101-0539) and ZnS (96-110-0044). The diffraction patterns are shown in Figure 3a, while the enlarged and normalized profiles of the (111) reflection are presented in Figure 3b.

The peak position shifted toward higher 2θ values across the sample series. The lattice constants obtained from the (111) reflection were 6.081, 6.057, 6.014, and 5.914 Å for substrate temperatures of 100, 150, 200, and 250 $°C$, respectively. The corresponding FWHM values were 0.2019°, 0.2303°, 0.2814°, and 0.1791°, while the calculated crystallite sizes were 40.4, 25.9, 17.4, and 34.7 nm, respectively. The largest crystallite size was obtained for the film deposited at 100 $°C$ (40.4 nm), followed by the film deposited at 250 $°C$ (34.7 nm), whereas the minimum value was observed at 200 $°C$ (17.4 nm).

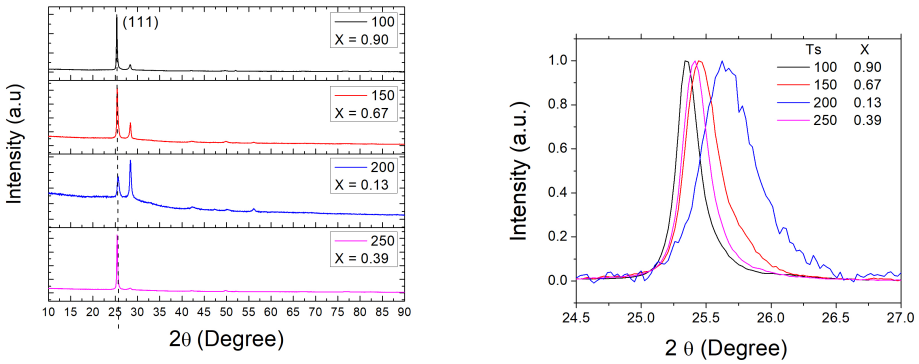

(a) (b)

Fig. 3: X-ray diffraction analysis of $ZnS_{1-x}Te_x$ thin films deposited at different substrate temperatures and Te fractions. (a) XRD patterns showing the predominantly cubic zinc-blende structure. (b) Enlarged and normalized profiles of the (111) reflection, showing the variation in peak position and width across the sample series.

3.3 Optical characterization

The transmittance spectra of the $ZnS_{1-x}Te_x$ thin films deposited at different substrate temperatures are shown in Figure 4a. The films exhibited a transparent region approximately between 650 and 2500 nm and a high-absorption region between 300 and 650 nm. The spectral position of the absorption edge varied substantially among the films deposited at different substrate temperatures.

The refractive index and absorption coefficient were obtained from the transmittance spectra using Swanepoel's method. The spectral dependence of the refractive index is shown in Figure 4b, while the absorption coefficient spectra are presented in Figure 4c. At wavelengths below 600 nm, all films exhibited high absorption coefficients of the order of $10^4\,\mathrm{cm}^{-1}$.

The optical band gap was determined by extrapolating the linear region of the $(\alpha h\nu)^2$ versus $h\nu$ plots to the energy axis (Figure 4d). The band-gap energies were 2.19, 2.19, 2.56, and 3.13 eV for films deposited at 100, 150, 200, and 250 °C, corresponding to Te concentrations $x = 0.90$, 0.67, 0.13, and 0.39, respectively.

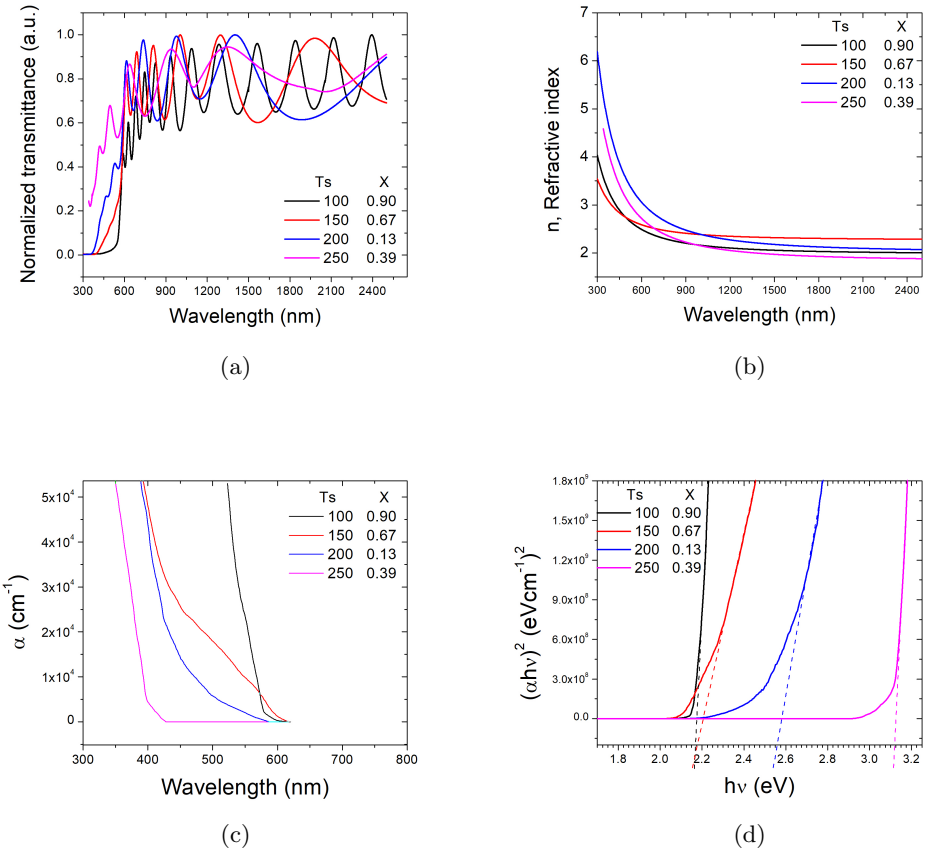

Fig. 4: Optical properties of $ZnS_{1-x}Te_x$ thin films deposited at different substrate temperatures and Te fractions. (a) Optical transmittance spectra. (b) Spectral dependence of the refractive index determined using Swanepoel's method. (c) Absorption coefficient spectra. (d) Tauc plots, $(\alpha h\nu)^2$ versus $h\nu$, used to determine the direct optical band-gap energy.

3.4 Photoluminescence

The photoluminescence spectrum of the film deposited at 100 °C ($x = 0.90$) exhibited a broad emission band (Figure 5). Fitting the spectrum with two Gaussian components yielded maxima at 515 and 579 nm.

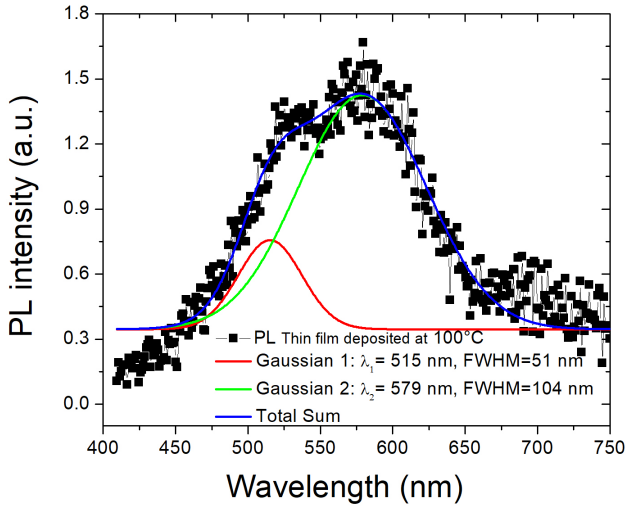

Fig. 5: Room-temperature photoluminescence spectrum of the $ZnS_{0.10}Te_{0.90}$ thin film deposited at 100 °C. The experimental spectrum is shown together with the two Gaussian components centered at approximately 515 and 579 nm and their cumulative fit.

3.5 Photoconductivity

The photoconductivity spectra of the $ZnS_{1-x}Te_x$ thin films showed broad spectral responses that depended on substrate temperature (Figure 6). Films deposited at 100 and 150 °C exhibited a photocurrent response over almost the entire visible range, with maxima near 550 nm. The film deposited at 200 °C also showed a maximum near 550 nm, but its spectral response was mainly restricted to approximately 400–650 nm. The film deposited at 250 °C exhibited its maximum near 600 nm and a broader response extending approximately from 525 to 800 nm. Contributions at wavelengths above 600 nm were observed for the films deposited at 100, 150, and 250 °C.

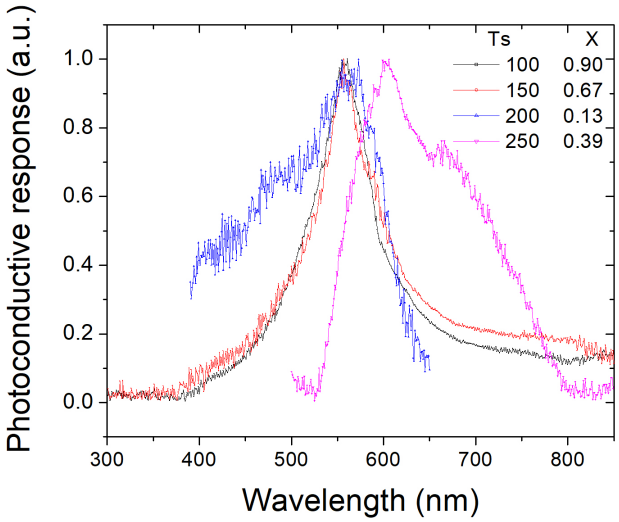

Fig. 6: Spectral photoconductivity responses of $ZnS_{1-x}Te_x$ thin films deposited on glass substrates at different substrate temperatures and Te fractions.

4 Discussion

4.1 Composition of the ternary $ZnS_{1-x}Te_x$ thin films

The EDX measurements reveal a pronounced influence of substrate temperature on the final S/Te ratio of the co-evaporated $ZnS_{1-x}Te_x$ films. The Te fraction decreases from $x = 0.90$ at 100 °C to $x = 0.13$ at 200 °C, followed by an increase to $x = 0.39$ at 250 °C. Consequently, despite using the same nominal amounts of ZnS and ZnTe for all depositions, the resulting alloy composition does not vary monotonically with substrate temperature. This indicates that the amount of S and Te incorporated into the growing films is sensitive to the deposition conditions.

A strong influence of substrate temperature on growth rate, morphology, crystalline quality, and optical properties has previously been reported for thermally evaporated ZnTe films [10]. In the present case, temperature-dependent incorporation or re-emission of S- and Te-containing species could contribute to the compositional evolution, particularly to the increase in Te content observed at 250 °C. The available measurements, however, do not allow the microscopic origin of this reversal to be established because sticking coefficients, desorption rates, and surface kinetics were not measured directly.

4.2 Structural characterization

The XRD patterns show that the $ZnS_{1-x}Te_x$ films are polycrystalline and predominantly retain the cubic zinc-blende structure, with a strong contribution from the

(111) reflection. Similar structural characteristics have been reported for thermally evaporated ZnTe and ZnS films. Prakash et al. [2] observed polycrystalline cubic zinc-blende structures in ZnTe and ZnS films deposited on glass, while Bacaksiz et al. [10] reported a strong (111) texture in evaporated zinc-blende ZnTe films. These observations are consistent with the structural assignment of the present ternary films.

Across the sample series, the (111) reflection shifts toward higher 2θ values, accompanied by a decrease in the calculated lattice constant from 6.081 Å at 100 °C to 5.914 Å at 250 °C. A contraction of the lattice is qualitatively expected as smaller S atoms replace Te atoms in a Te-rich environment. The EDX and XRD trends, however, are not strictly parallel. Although the film deposited at 250 °C contains more Te than the 200 °C film, it exhibits a smaller lattice constant. Average composition alone is therefore insufficient to account for the structural evolution of the entire series. Local relaxation, strain, alloy disorder, and differences in crystallite growth may also influence the measured lattice parameter. The increase in crystallite size from 17.4 nm at 200 °C to 34.7 nm at 250 °C further illustrates that substrate temperature affects the microstructure in addition to the final alloy composition.

4.3 Optical characterization

The interference fringes in the transmittance spectra arise from constructive and destructive interference at the film interfaces, while the displacement of the absorption edge among the samples reflects substantial changes in their optical response. Swanepoel's envelope method, used here to extract the optical constants, has previously been applied to thermally evaporated ZnTe and ZnS films [2]. All samples exhibit absorption coefficients of the order of 10^4 cm^{-1} below approximately 600 nm, characteristic of strong optical absorption in direct-gap II–VI semiconductor films.

Interpreting the measured band gaps requires particular care because $ZnS_{1-x}Te_x$ does not follow a simple linear interpolation between the ZnS and ZnTe end members. Yu et al. [6] reported pronounced band-gap bowing in $ZnS_{1-x}Te_x$ epilayers, described at room temperature by $E_g(x) = 3.73 - 5.27x + 3.80x^2$, where x is the Te fraction. An anomalous composition dependence was also reported by Seong et al. [7], who discussed the influence of alloy composition and local atomic arrangements.

Our films show the same general complexity rather than a monotonic composition–gap relationship. E_g is 2.19 eV for both Te-rich samples ($x = 0.90$ and 0.67), increases to 2.56 eV at $x = 0.13$, and reaches 3.13 eV for the $x = 0.39$ film. The measurements therefore establish substantial optical-gap tunability but do not support a simple one-to-one dependence of E_g on the average Te concentration. Composition, local alloy configuration, strain, structural disorder, and defect-related states may contribute simultaneously to the measured optical response. In this regard, Zhang et al. [13] showed that sulfur incorporation into ZnTe can introduce electronic states within the band gap, illustrating how changes in local composition can modify the electronic structure of $ZnS_{1-x}Te_x$.

4.4 Photoluminescence

The room-temperature PL spectrum of the Te-rich film ($x = 0.90$) is broad and can be represented by two Gaussian components centered at approximately 515 and 579 nm. Such a spectrum points to the contribution of more than one radiative recombination channel, although the present measurement alone does not identify their microscopic origin. Composition-dependent luminescence has been reported previously for $ZnS_{1-x}Te_x$: Yu et al. [6] observed room-temperature emission extending from the blue to the yellow region, with the PL peak shifting toward lower energies as the Te concentration increased. Sulfur-related localized states are also relevant in this alloy system. Ge et al. [14] identified S isoelectronic centers in a ZnTe matrix associated with deep-level luminescence, while Zhang et al. [13] reported S-induced states within the ZnTe band gap.

These observations provide possible physical contexts for the broad emission measured here, but they do not justify assigning either Gaussian component to a unique recombination mechanism. In particular, attributing the 579 nm component exclusively to ZnTe and the 515 nm component exclusively to the ternary alloy would require additional evidence. Temperature- or excitation-dependent PL, together with complementary defect-sensitive measurements, would be needed to distinguish more reliably between band-to-band, localized-exciton, and defect-related recombination.

4.5 Photoconductivity

The most evident change in the photoconductivity spectra occurs in their wavelength dependence. Films deposited at 100 and 150 °C respond over almost the entire visible range and exhibit maxima near 550 nm. The 200 °C film retains a maximum near 550 nm, but its response is mainly confined to approximately 400–650 nm. At 250 °C, the maximum shifts to about 600 nm and the response extends from approximately 525 to 800 nm. These spectral changes accompany the variations in composition, absorption edge, band-gap energy, and structural properties observed across the same sample series.

Of particular interest is the photocurrent detected above 600 nm for the films deposited at 100, 150, and 250 °C. When the corresponding photon energy lies below the measured optical gap, direct band-to-band excitation alone cannot account for this part of the response. Localized or defect-related states offer one possible route for sub-gap photoexcitation, especially considering the sulfur-related states previously identified in ZnTe-based alloys [13, 14]. This interpretation remains tentative, since the present measurements do not resolve the electronic states responsible for the long-wavelength photocurrent.

Previous work nevertheless establishes that the $ZnS_{1-x}Te_x$ system can be used for photodetection. Sou et al. [9] fabricated $ZnS_{1-x}Te_x$-based Schottky photovoltaic detectors with composition-dependent spectral sensitivity and reported external quantum efficiencies above 50% for a low-Te device grown on GaP. Direct performance

comparison with those epitaxial devices would not be appropriate for the present polycrystalline co-evaporated films. Here, the relevant result is the ability to modify the spectral photoconductive response through the deposition conditions and the accompanying changes in alloy composition. Establishing the actual detector performance of these films will require measurements of responsivity, specific detectivity, dark current, noise, temporal response, and stability.

5 Conclusions

$ZnS_{1-x}Te_x$ thin films were successfully grown on glass substrates by thermal co-evaporation at substrate temperatures between 100 °C and 250 °C. Although identical nominal amounts of ZnS and ZnTe were used for all depositions, the Te fraction varied markedly across the sample series, from $x = 0.90$ at 100 °C to $x = 0.13$ at 200 °C, followed by an increase to $x = 0.39$ at 250 °C. Substrate temperature therefore emerges as an important growth parameter influencing the final composition of the films rather than producing a simple monotonic variation in Te incorporation.

The compositional changes were accompanied by substantial modifications in the structural and optical properties. All films remained predominantly polycrystalline with a cubic zinc-blende structure and preferred (111) orientation, while the lattice constant decreased from 6.081 to 5.914 Å across the investigated temperature range. The optical band gap varied between 2.19 and 3.13 eV without following a simple monotonic dependence on the measured Te fraction, consistent with the complex composition dependence reported for the $ZnS_{1-x}Te_x$ alloy system. The broad PL emission observed for the Te-rich film and the changes in the photoconductivity spectra further indicate that the optoelectronic behavior cannot be described solely in terms of average alloy composition.

Most notably, the spectral photoconductive response could be modified through the deposition conditions. Films grown at 100 and 150 °C exhibited broad sensitivity over almost the entire visible region, whereas the film deposited at 250 °C showed a red-shifted maximum near 600 nm and a response extending to approximately 800 nm. Taken together, these results establish a clear connection between growth conditions, alloy composition, and the optoelectronic response of co-evaporated $ZnS_{1-x}Te_x$ thin films. This tunability makes the system worthy of further investigation for broadband visible photodetection, although responsivity, specific detectivity, dark current, noise, temporal response, and device stability must still be quantified before its performance can be assessed against established photodetector technologies.

Acknowledgments

The authors gratefully acknowledge the Grupo de Materiales con Aplicaciones Tecnológicas (GMAT) at the Universidad Nacional de Colombia (UNAL) for providing the facilities and support required for the preparation of the thin films studied in this work. The authors also thank the Department of Physics at UNAL for providing access to the specialized instrumentation and facilities used for the structural and optical

characterization of the samples, including X-ray diffraction and spectrophotometric measurements. Their institutional and technical support was essential for carrying out the experimental work presented in this study.

Declarations

Funding

The authors declare that no funds, grants, or other support were received for conducting this study or preparing this manuscript.

Competing interests

The authors have no relevant financial or non-financial interests to disclose.

Ethics approval and consent to participate

Not applicable.

Consent for publication

Not applicable.

Data availability

The datasets generated and/or analyzed during the current study are available from the corresponding author on reasonable request.

Materials availability

Not applicable.

Code availability

Not applicable.

Author contributions

Camilo Andrés Velásquez Andrade: Conceptualization, experimental work, methodology, data analysis, and writing of the original manuscript.
Néstor Jaime Torres: Conceptualization, supervision, and critical review of the manuscript.

References

[1] Klingshirn, C.F.: Optical Properties of Bound and Localized Excitons and of Defect States, pp. 363–382. Springer, Berlin, Heidelberg (2012). https://doi.org/10.1007/978-3-642-28362-8_14

[2] Prakash, D., Aboraia, A.M., El-Hagary, M., Shaaban, E.R., Verma, K.D.: Determination of the optical constants and film thickness of ZnTe and ZnS thin films in terms of spectrophotometric and spectroscopic ellipsometry. Ceramics International **42**(2), 2676–2685 (2016) https://doi.org/10.1016/j.ceramint.2015.10.096

[3] Kishino, M., Tanaka, S., Senda, K., Yamada, Y., Taguchi, T.: Photoluminescence characterization of MBE-grown $ZnTe_xSe_{1-x}$ epitaxial layers with high Te concentrations. Journal of Crystal Growth **214–215**, 220–224 (2000) https://doi.org/10.1016/S0022-0248(00)00089-0

[4] Nagarethinam, V.S., Ahamed, M.G.S.B., Vijayakumar, K., Amalraj, L., Balu, A.R., Thayumanavan, A., Murali, K.R., Sanjeeviraja, C., Jayachandran, M.: Structural, optical and electrical properties of $ZnTe_{1-x}Se_x$ thin films. Journal of Materials Science: Materials in Electronics **22**(6), 607–613 (2011) https://doi.org/10.1007/s10854-010-0185-9

[5] Suthagar, J., Suthan Kissinger, N.J., Balasubramaniam, M., Perumal, K.: Photoluminescence properties of $ZnSe_{1-x}Te_x$ thin films on GaAs/ITO substrates by electron beam evaporation technique. Science China Technological Sciences **54**(1), 52–57 (2011) https://doi.org/10.1007/s11431-010-4186-y

[6] Yu, Y.-M., Nam, S., Oh, B., Lee, K.-S., Choi, Y.D., Lee, J., Yu, P.Y.: Variation of band gap energy and photoluminescence characteristics with Te composition of ZnS1-xTex epilayers grown by hot-wall epitaxy. Applied Surface Science **182**(1-2), 159–166 (2001) https://doi.org/10.1016/S0169-4332(01)00550-5

[7] Seong, M.J., Alawadhi, H., Miotkowski, I., Ramdas, A.K., Miotkowska, S.: The anomalous variation of band gap with alloy composition: cation vs anion substitution in ZnTe. Solid State Communications **112**(6), 329–334 (1999) https://doi.org/10.1016/S0038-1098(99)00356-7

[8] Sou, I.K., Mao, J., Ma, Z., Chen, W.S., Yang, Z., Wong, K.S., Wong, G.K.L.: Blue-light emission from ZnSTe-based EL devices. Journal of Crystal Growth **175–176**, 632–636 (1997) https://doi.org/10.1016/S0022-0248(96)01002-0

[9] Sou, I.K., Man, C.L., Ma, Z.H., Yang, Z., Wong, G.K.L.: High performance ZnSTe photovoltaic visible-blind ultraviolet detectors. Applied Physics Letters **71**(26), 3847–3849 (1997) https://doi.org/10.1063/1.120522

[10] Bacaksiz, E., Aksu, S., Ozer, N., Tomakin, M., Ozcelik, A.: The influence of substrate temperature on the morphology, optical and electrical properties of thermal-evaporated ZnTe thin films. Applied Surface Science **256**(5), 1566–1572 (2009) https://doi.org/10.1016/j.apsusc.2009.09.023

[11] Scherrer, P.: Bestimmung der inneren Struktur und der Größe von Kolloidteilchen mittels Röntgenstrahlen, pp. 387–409. Springer, Berlin, Heidelberg (1912). https:

//doi.org/10.1007/978-3-662-33915-2_7

[12] Swanepoel, R.: Determination of the thickness and optical constants of amorphous silicon. Journal of Physics E: Scientific Instruments **16**(12), 1214–1222 (1983) https://doi.org/10.1088/0022-3735/16/12/023

[13] Zhang, X., Xu, M., Li, Q., Wang, M., Akhmadaliev, S., Zhou, S., Wu, Y., Guo, B.: Optical properties of ZnSxTe1-x synthesized by sulfur implantation. Nuclear Instruments and Methods in Physics Research Section B: Beam Interactions with Materials and Atoms **442**, 24–27 (2019) https://doi.org/10.1016/j.nimb.2018.12.002

[14] Ge, W.K., Lam, S.B., Sou, I.K., Wang, J., Wang, Y., Li, G.H., Han, H.X., Wang, Z.P.: Sulfur forming an isoelectronic center in zinc telluride thin films. Physical Review B **55**(15), 10035–10039 (1997) https://doi.org/10.1103/PhysRevB.55.10035